Solution NMR Structures of IgG Binding Domains with Artificially Evolved High Levels of Sequence Identity but Different Folds[†,‡]

Yanan He, Deok Cheon Yeh, Patrick Alexander, Philip N. Bryan, and John Orban*

Center for Advanced Research in Biotechnology, University of Maryland Biotechnology Institute, 9600 Gudelsky Drive, Rockville, Maryland 20850

Received June 27, 2005; Revised Manuscript Received August 26, 2005

ABSTRACT: We describe here the solution NMR structures of two IgG binding domains with highly homologous sequences but different three-dimensional structures. The proteins, G311 and A219, are derived from the IgG binding domains of their wild-type counterparts, protein G and protein A, respectively. Through a series of site-directed mutations and phage display selections, the sequences of G311 and A219 were designed to converge to a point of high-level sequence identity while keeping their respective wild-type tertiary folds. Structures of both artificially evolved sequences were determined by NMR spectroscopy. The main chain fold of G311 can be superimposed on the wild-type α/β protein G structure with a backbone rmsd of 1.4 Å, and the A219 structure can be overlaid on the wild-type three-α-helix protein A fold also with a backbone rmsd of 1.4 Å. The structure of G311, in particular, accommodates a large number of mutational changes without undergoing a change in the overall fold of the main chain. The structural differences are maintained despite a high level (59%) of sequence identity. These proteins serve as starting points for further experiments that will probe basic concepts of protein folding and conformational switching.

Understanding the relationship between protein sequence and three-dimensional structure remains one of the fundamental unsolved problems in structural biology. The identification of key amino acids that stabilize a particular fold in preference to alternative folds would therefore provide insights useful for both protein design and fold-prediction algorithms. Several previous studies have approached the folding problem by reducing the sequence differences between proteins with different structures (*1*−*3*). While each of these studies was informative, the most successful at deriving two different, stable structures with a high degree of sequence identity came from the Regan laboratory. They initially reported a stable mutant that was 50% identical to the IgG binding domain of protein G but maintained the fold of a RNA binding protein ROP-like dimer (*4*, *5*). In a subsequent study, they showed that even higher levels of sequence identity were possible, although these tended to be either less stable or more prone to aggregation (*6*).

A combination of computational modeling and intuition was used in the above cases to guide the selection of mutants in the protein design process. In contrast, we present in the accompanying paper a novel strategy using primarily genetic selection methods for designing two mutant proteins with a high level of sequence identity but with different stable folds (P. Alexander et al., accompanying paper). These proteins, termed G311 and A219, are mutants of the IgG binding domains of protein G and protein A, respectively. The protein G IgG binding domains (herein termed protein G or G_B) are small 56-amino acid polypeptides from streptococcal species of Lancefield group G that have an α/β fold consisting of a four-stranded β-sheet packed against an α-helix (*7*−*11*). The IgG binding domains of protein A (herein termed protein A or A_B) are from *Staphylococcus aureus*, contain 58 residues, and have a three-helix bundle (3-α) fold (*12*−*14*). The wild-type sequences of G_{B2} (one of two to three G_B domains depending on the strain) and A_B have only nine identical residues. A total of 21 mutations were introduced in converting G_{B2} to G311, while nine mutations were introduced in going from A_B to A219. As a result of selection for these mutations, G311 and A219 have a total of 33 identical residues out of 56.

In this paper, we describe the detailed three-dimensional solution NMR structures of G311 and A219. We evaluate the structural consequences of these mutations and demonstrate that, despite the high degree of sequence identity (59%), G311 and A219 are stable and monomeric and maintain their respective wild-type folds. These proteins serve as useful starting points for further studies on the α/β versus 3-α folding preferences of G311 mutants from the 23 nonidentical amino acids.

MATERIALS AND METHODS

NMR Spectroscopy. Details of the cloning, expression, and purification of G311 and A219 are provided in the accompanying manuscript by P. Alexander et al. ^{15}N-labeled and $^{13}C/^{15}N$-labeled NMR samples of both proteins were prepared at a concentration of 0.2−0.4 mM in 100 mM

[†] Supported by NIH Grant GM62154.

[‡] The coordinates for G311 and A219 have been deposited in the Protein Data Bank as entries 1zxh and 1zxg, respectively. Chemical shift assignments for G311 and A219 have been deposited in BioMagResBank as entries BMRB-6679 and BMRB-6680, respectively.

* To whom correspondence should be addressed. Phone: (240) 314-6221. Fax: (240) 314-6255. E-mail: orban@umbi.umd.edu.

10.1021/bi051232j CCC: $30.25
Published on Web 09/28/2005

Table 1: Summary of Protein Design Steps for G311 and A219

design step	positions changed or randomized	G_B to A_B (G311) net mutations	A_B to G_B (A219) net mutations
(1) first part of A_B IgG binding cassette	13, 14, 17	K13F, G14Y, T17L	
(2) phage selection for β-sheet surface	2, 4, 6, 8, 19, 42, 44, 46, 51, 53, 55	T2Y, K4L, N8K, T55Q	
(3) phage selection for interior residues	5, 7, 9−12, 33, 34, 38, 41, 54, 56	L5V, I7N, K10Q, T11N, L12A, Y33S, A34L, E56A	
(4) rest of A_B IgG binding cassette	27, 28, 31, 35, 37, 40	E27R, K28N, K31I, N35K, N37D, D40Q	
(5) place optimized N-terminus of G_B into A_B	1−8		D2Y, N3Y, K4L, F5V, N6V, K7N, E8K
(6) additional mutations	29, 54		G29A, A54V

potassium phosphate buffer at pH 7 with 10% D_2O added. Spectra were acquired on a Bruker DRX-600 instrument equipped with a *z*-axis gradient triple-resonance cryoprobe. ^{15}N HSQC spectra of G311 were recorded over a temperature range of 2−25 °C, and data for structure determination were acquired at 2 °C. All experiments on A219 were conducted at 25 °C. Data were processed on a Linux workstation using nmrPipe (*15*) and analyzed using Sparky (T. D. Goddard and D. G. Kneller, University of California, San Francisco). NMR assignments were made using standard triple-resonance experiments (*16*−*21*). Backbone resonances were obtained from HNCACB, CBCA(CO)NH, and HNCO spectra. Side chain assignments were made from HBHA(CO)NH, (H)C(CO)NH-TOCSY, H(CCO)NH-TOCSY, 3D ^{15}N-TOCSY, and NOESY spectra. Interproton NOEs were obtained from 3D ^{15}N NOESY (*22*) and aliphatic and aromatic 3D ^{13}C NOESY (*23*) spectra with mixing times of 100 and 150 ms.

Structure Calculations and Analysis. Structures were calculated initially from an extended polypeptide chain using CNS 1.1 (*24*) and standard simulated annealing and torsion angle dynamics protocols. Initial NOE restraints were generated automatically using NOEID, an in-house NOE assignment program (http://orban.umbi.umd.edu/NOEID). After this initial assignment step using NOEID, further assignments were done manually in a semi-automated fashion using NOEID and intermediate structures to iteratively narrow down ambiguous assignments. Distance restraints based on peak intensities were categorized as strong (1.8−3.0 Å), medium (1.8−4.0 Å), weak (1.8−5.5 Å), and very weak (2.8−6.0 Å). Backbone dihedral angle restraints were obtained on the basis of chemical shift values using TALOS (*25*). Two restraints were used to define each hydrogen bond, 1.5−2.5 Å for r_{HN-O} and 2.3−3.2 Å for r_{N-O}, and these restraints were used only in the later stages of refinement. Nonbonded contacts were represented by a quartic van der Waals repulsion term. Final values for force constants were 1000 kcal mol^{-1} $Å^{-2}$ for bond lengths, 500 kcal mol^{-1} rad^{-2} for angles and improper torsions, 40 kcal mol^{-1} $Å^{-2}$ for experimental distance restraints, 200 kcal mol^{-1} rad^{-2} for dihedral angle restraints, and 4.0 kcal mol^{-1} $Å^{-4}$ for the van der Waals repulsion term. The 20 best structures for each protein were chosen on the basis of a low total energy, no NOE distance violations greater than 0.30 Å, no dihedral restraint violations greater than 5°, and standard indicators of structure quality as shown in Table 2. Structures were analyzed using PROCHECK-NMR (*26*), MolProbity (*27*), and QUANTA (Molecular Simulations Inc.) and displayed using MOLMOL (*28*).

Table 2: Statistics for the G311 and A219 Ensembles of 20 Structures

	A219	G311
experimental restraints		
no. of NOE restraints		
all NOEs	1075	1082
intraresidue	571	585
sequential ($\|i-j\|=1$)	218	232
medium-range ($1<\|i-j\|\leq 5$)	166	116
long-range ($\|i-j\|>5$)	120	149
no. of hydrogen bond restraints	46	64
no. of dihedral angle restraints	70	77
total no. of restraints	1191	1223
rmsds from the mean structure (Å)		
over all residues[a]		
backbone atoms	0.31 ± 0.10	0.31 ± 0.10
heavy atoms	1.08 ± 0.15	1.28 ± 0.25
secondary structures[b]		
backbone atoms	0.25 ± 0.10	0.28 ± 0.09
heavy atoms	1.04 ± 0.17	1.33 ± 0.28
measures of structure quality		
Ramachandran distribution		
most favored regions (%)	82.0 ± 2.8	76.2 ± 1.0
additionally allowed regions (%)	9.5 ± 2.6	21.4 ± 1.1
generously allowed regions (%)	4.2 ± 2.0	0.6 ± 0.9
disallowed regions (%)	4.4 ± 1.3	2.0 ± 0.0
no. of bad contacts/100 residues	7.7 ± 1.6	3.7 ± 1.4
overall dihedral *G* factor	0.1 ± 0.0	−0.06 ± 0.02
Cβ deviation (Å)	0.01−0.16	0.01−0.09

[a] For G311, residues 1−56. For A219, residues 8−56. [b] The secondary elements used were as follows: A219, residues 9−17, 25−36, and 41−54; G311, residues 1−8, 13−18, 22−37, 41−46, and 51−56.

RESULTS

Protein Design. The G311 and A219 sequences were converged using a combination of site-directed mutagenesis and phage selection methods. The latter approach permitted an extensive search of sequence space at the designated positions in the sequence. A comprehensive description of the experiments used to generate the G311 and A219 proteins is provided in the accompanying paper by P. Alexander et al., and a summary of the design steps is presented here (Table 1 and Figure 1). A total of 21 mutations were introduced in going from wild-type G_{B2} to G311. First, part of the A_B IgG binding cassette was introduced into G_{B2}. The resulting three-residue K13F/G14Y/T17L mutant is stable and has the additional useful property of abolishing any detectable binding to the Fab (*29*) while maintaining binding to IgG Fc. Second, the surface residues on the β-sheet were optimized using a phage selection method. Residues in strand β1 were randomized among 12 possible amino acid types, whereas surface residues in strands β2−β4 were selected from either A_B or G_B amino acids. Third, internal sites in the protein were randomized using phage selection. Again,

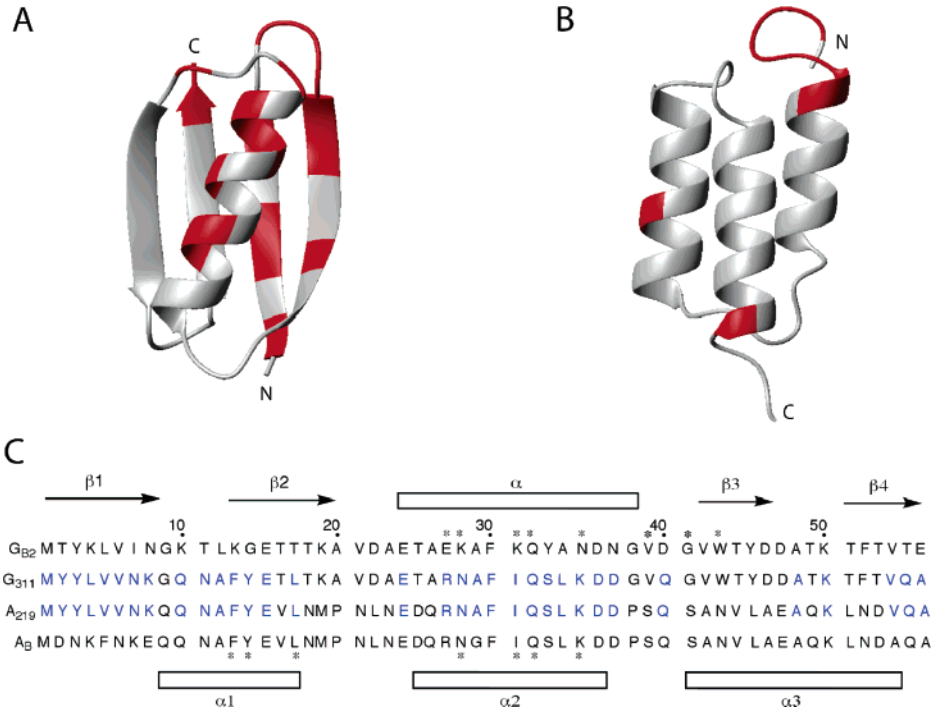

FIGURE 1: (A) Ribbon diagram of the wild-type protein G (G_B) structure highlighting in red residues that were mutated in the design of the G311 protein. (B) Ribbon diagram of the wild-type protein A (A_B) structure. Residues mutated to make A219 are colored red. (C) Sequence alignment of G_{B2}, G311, A219, and A_B. Identities between G311 and A219 are colored blue. The secondary structure elements of G_{B2} and A_B are displayed above and below the sequences, respectively. IgG binding epitopes for G_{B2} and A_B are indicated with asterisks.

residues in strand β1 were optimized from among 12 possible amino acid types, and the remaining sites were allowed to be either the A_B or G_B amino acids. In both rounds of phage display, the native α/β fold was selected by detecting binders to IgG since the G_B-type IgG binding epitope is still intact. Once the internal and surface residues were optimized, the remainder of the A_B-type IgG binding cassette was introduced to provide the final G311 sequence. Thus, G311 cannot bind to IgG in the α/β conformation but will bind to IgG if the conformation is switched to the A_B 3-α fold since a cryptic A_B IgG binding site is present in the G311 sequence.

The A219 sequence was derived from A_B via nine mutations (Table 1). Residues 2−8 were replaced with the optimized strand β1 sequence from G311. In addition, two other mutations, G29A and A54V, were introduced at solvent accessible sites to replace A_B residues with G_B amino acids.

NMR Assignment and Structure of G311. Both size exclusion chromatography and concentration-dependent thermal melting monitored by CD spectroscopy indicated that G311 is monomeric (P. Alexander et al., accompanying paper). ^{15}N HSQC spectra recorded over the temperature range of 2−25 °C showed that several peaks, in particular, those due to residues in strands β1 and β2 (N7, K8, Y14, T16, and L17), were broadened at 25 °C, suggesting conformational exchange at this temperature. Spectra for structure determination were therefore acquired at 2 °C where all of the expected amide cross-peaks were readily detected (Figure 2A). Further studies on dynamics in this system are in progress and will be described elsewhere. NMR assignments were made for nearly all backbone amides (except Q10) and approximately 90% of the side chain protons. The G311 structure consists of four β-strands, β1 (residues 3−8), β2 (residues 12−18), β3 (residues 42−46), and β4 (residues 51−56), and one α-helix (residues 24−38). The arrangement of the secondary structure elements is β1-β2-α-β3-β4, and the four β-strands form a β-sheet with a strand order of 2143. A superposition of main chains for the 20 lowest-energy structures is shown in Figure 3A, and an overlay of core residues is displayed in Figure 3B. The average backbone rmsd for this ensemble is 0.31 ± 0.10 Å, and the rmsd per residue for backbone atoms is provided in Figure 4A. The complete list of structure statistics is given in Table 2.

NMR Assignment and Structure of A219. The oligomeric state of A219 was determined to be monomeric on the basis of size exclusion chromatography and concentration-dependent thermal melting characteristics (P. Alexander et al., accompanying paper). NMR assignments were made at 25 °C for all backbone amides of A219 and more than 90% of all side chain protons. NOE data analysis indicated that the structure contains three amphipathic α-helices, α1 (residues 9−17), α2 (residues 25−36), and α3 (residues 41−54), arranged in a compact bundle. The three α-helices are well ordered with the loop region between α2 and α3 being less well-defined (Figure 4B). The first eight residues have few inter-residue NOEs and form a disordered N-terminal tail, while residues 55−58 at the C-terminus are also poorly defined. Figure 5A shows a backbone overlay of the 20 lowest-energy structures with an average backbone rmsd for residues 8−56 of 0.31 ± 0.10 Å. The side chains in the core of the protein are also well ordered, reflecting numerous NOE contacts (Figure 5B). Complete structure statistics are given in Table 2.

DISCUSSION

Structural Consequences of Mutations in G311. Of the 56 residues in protein G, 21 positions were mutated in going from the wild-type G_{B2} sequence to G311. This represents a significant change in sequence (37.5%), and so three-

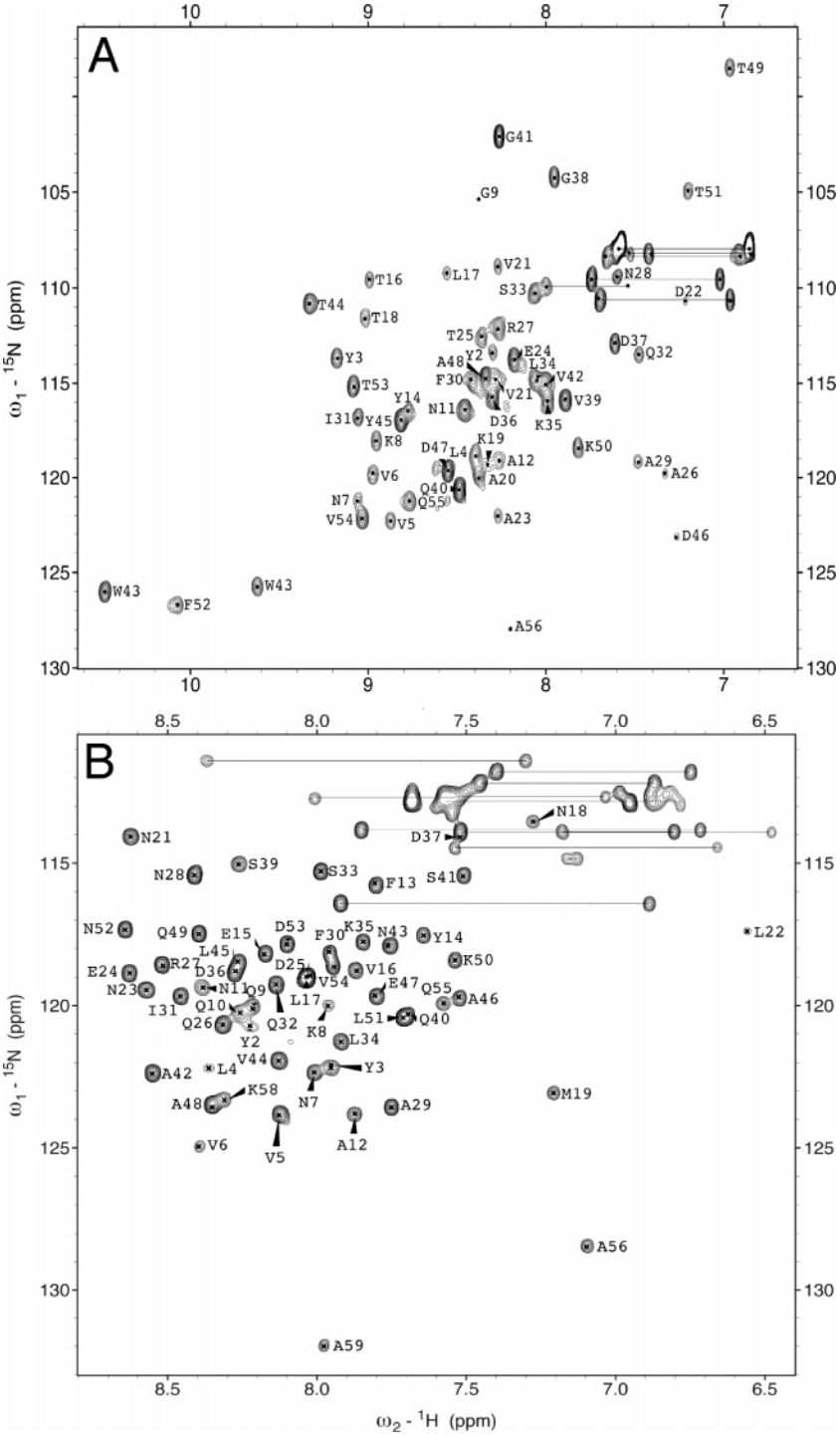

FIGURE 2: (A) ^{15}N HSQC spectrum of G311 at 2 °C. (B) ^{15}N HSQC spectrum of A219 at 25 °C. Main chain amide assignments are shown in both spectra.

dimensional structure determination of G311 was essential in confirming that the native α/β fold was maintained. Although a large number of mutations were made, the overall fold of G311 agrees well with the structures reported in the literature for wild-type protein G. In particular, the backbone rmsd between G311 and the 1.1 Å X-ray structure of G_B [PDB entry 1igd (*11*)] is 1.4 Å. A similar rmsd value of 1.5 Å is obtained when comparing G311 with the NMR structure of G_{B1} [PDB entry 2gb1 (*7*)]. The hydrophobic core of G311 is well packed and shares similarities with the wild-type structure. There are, however, a number of differences due directly to mutation or a result of indirect effects on conserved residues. The positions of residues in the core and in the boundary region between the core and surface are highlighted in Figure 6 and compared with their wild-type conformations.

Three mutations, L5V, I7N, and A34L, were introduced at positions that are completely buried in the hydrophobic core of the wild-type protein G structure. The L5V mutation is conservative and does not lead to significant conformational change in the core. The mutation from isoleucine to a polar asparagine at position 7 is allowed because this residue is no longer completely buried in G311 due to the L12A mutation. Substitution with a smaller side chain at residue

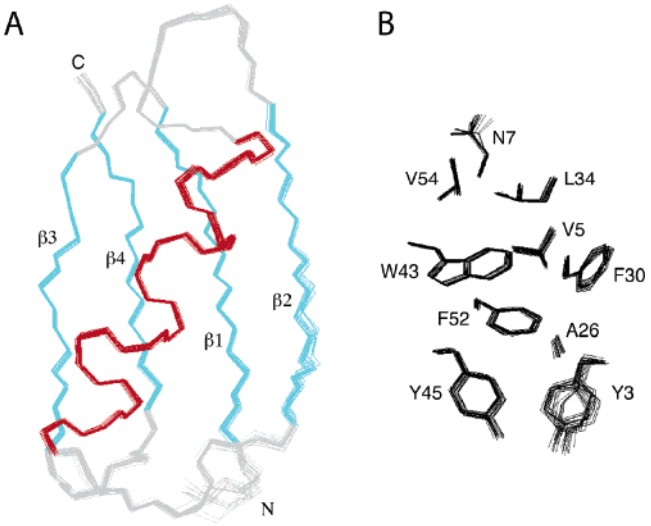

FIGURE 3: (A) Backbone superposition of the 20 lowest-energy structures for G311. β-Strand regions are highlighted in cyan, while the helix is colored red. (B) Overlay of G311 core residues in the 20-structure low-energy ensemble.

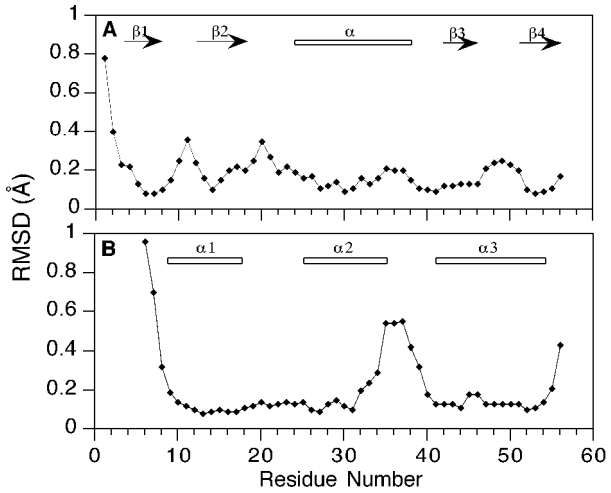

FIGURE 4: rmsd per residue for backbone atoms (N, C_α, and CO) in (A) G311 and (B) A219. Only rmsds of <1 Å are shown.

12 permits solvent access for N7. The asparagine side chain amide group is oriented toward the surface, while the methylene group points toward the hydrophobic core (Figures 3B and 6). At position 34, the phage-selected preference is for leucine (the A_B amino acid) over alanine (the G_B amino acid). The mutation to a significantly bulkier side chain is accommodated with some rearrangement of neighboring residues. Most notably, the W43 side chain is displaced from its wild-type conformation. In the wild-type structure, the A34 methyl group and the six-membered ring of the W43 indole group are in close contact. Placing the larger leucine side chain at position 34 is therefore likely to contribute, at least in part, to the reorientation of the W43 side chain in G311. The displacement of W43 from its wild-type position leads to further smaller changes in the positions of the neighboring residues, V54, F52, and F30 (Figure 6).

Five mutations, L12A, G14Y, K31I, Y33S, and N37D, were introduced at positions that are boundary residues in contact with the core. The A12 and D37 side chains occupy positions similar to those of their wild-type counterparts. The mutation of glycine to tyrosine at position 14 represents the

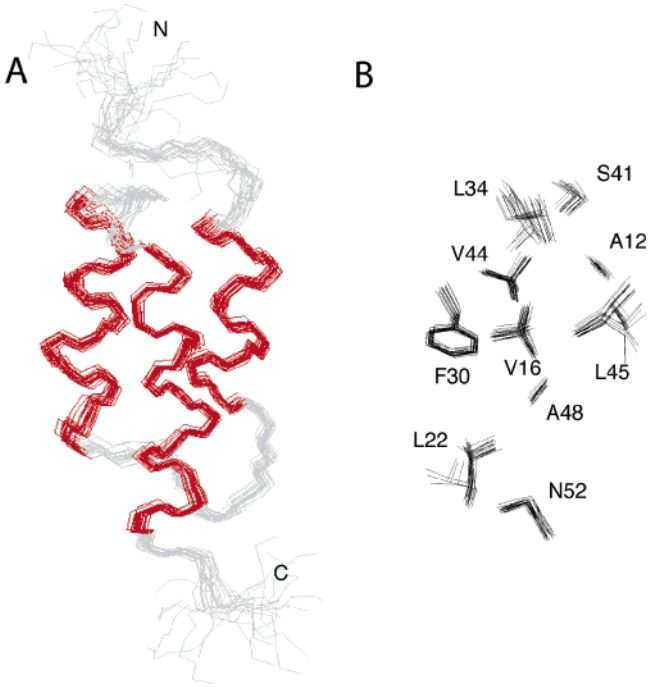

FIGURE 5: (A) Backbone superposition of the 20 lowest-energy structures for A219. Helical regions are highlighted in red. (B) Overlay of core residues in the 20-structure low-energy ensemble of A219.

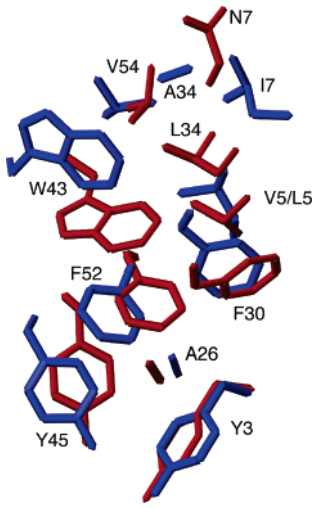

FIGURE 6: Comparison between core residue positions in G311 (red) and the X-ray structure of wild-type protein G (blue, PDB entry 1igd).

largest change in size for any single amino acid residue in G311 with eight added non-hydrogen atoms. Despite this large size difference, the Y14 residue is readily accommodated and reasonably well ordered in the ensemble of the 20 best structures. The conformation of Y14 appears to partly compensate for the Y33S mutation as these two tyrosine residues have overlapping packing interactions (Figure 7A). The G14Y mutation may therefore help to stabilize strand β2 and the overall fold of G311. The K31I mutation may contribute to the repositioning of W43, since the hydrophobic part of K31 packs against the indole ring of W43 in the wild-type protein G structure. In G311, the contacts between I31 and W43 are less extensive and I31 packs against the opposite face of the W43 indole ring (Figure 7B). The remaining 14 mutations in G311 (T2Y, K4L, N8K, K10Q,

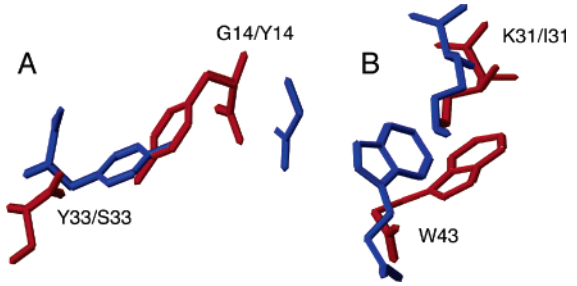

FIGURE 7: (A) Conformation of Y14 and S33 in G311 (red) compared with G14 and Y33 in the X-ray structure of wild-type G_B (blue, PDB entry 1igd). (B) Conformation of I31 and W43 in G311 (red) vs K31 and W43 in wild-type G_B (blue).

T11N, K13F, T17L, E27R, K28N, Y33S, N35K, D40Q, T55Q, and E56A) are at solvent accessible positions that do not significantly affect the packing of the core.

Structural Consequences of Mutations in A219. The overall fold of A219 is very similar to that of wild-type protein A [PDB entry 1q2n (*14*)] with an average backbone rmsd of 1.4 Å. The addition of the modified N-terminus (residues 1−8) does not affect the global fold since these residues do not adopt a regular structure. Moreover, since only solvent accessible residues were mutated (D2Y, N3Y, K4L, F5V, N6V, K7N, E8K, G29A, and A54V), the general core structure of A219 is similar to that of the native protein.

Structural Comparisons between G311 and A219. The sequences and secondary structure elements of G311 and A219 are summarized in Figure 1. These two proteins have 33 identical residues out of a 56-amino acid region of polypeptide chain, but despite this high level of sequence identity, G311 retains its wild-type α/*β* fold while A219 keeps its wild-type 3-α fold. For residues 1−20, the level of sequence identity is 75%. In G311, this region corresponds to a *β*1−*β*2 hairpin, whereas in A219, it encompasses a disordered N-terminus (residues 1−8) followed by an α-helix (residues 9−17). Residues 24−38 are helices for both G311 and A219 with a level of sequence identity of 80% in this central region. When these helices are superimposed, helix α1 of A219 overlays approximately with strand *β*4 of G311 while helix α3 of A219 aligns with strand *β*2 of G311 (Figure 8A). A comparison of the central helix backbone structures indicates that they are similar with an rmsd of 0.95 Å. However, the side chain conformations in the central helix vary from G311 to A219 for core residues such as F30 and L34, consistent with the different packing context of the respective α/*β* and 3-α folds (Figure 8B). Finally, residues 40−56 cover a *β*3−*β*4 hairpin in G311 but an α-helix in A219. This region has the lowest level of sequence similarity with a level of identity of 35%.

Relation to Other Studies. The fact that so many changes can be made to the G_B sequence without affecting the overall α/*β* fold is perhaps somewhat surprising in light of the demonstrated conformational plasticity of G_B when certain residues are mutated. In particular, the mutation of five core residues in G_{B1}, L5V, A26F, F30V, Y33F, and A34F, induces a large-scale rearrangement to an intertwined tetrameric structure with an altered hydrophobic core (*30*). Further mutagenesis experiments indicated that F26, V30, F34, and F52 are key for tetramer formation while F33 contributes to tetramer stability. In the preparation of G311, 21 mutations are introduced into G_{B2}. Two of the three core mutations,

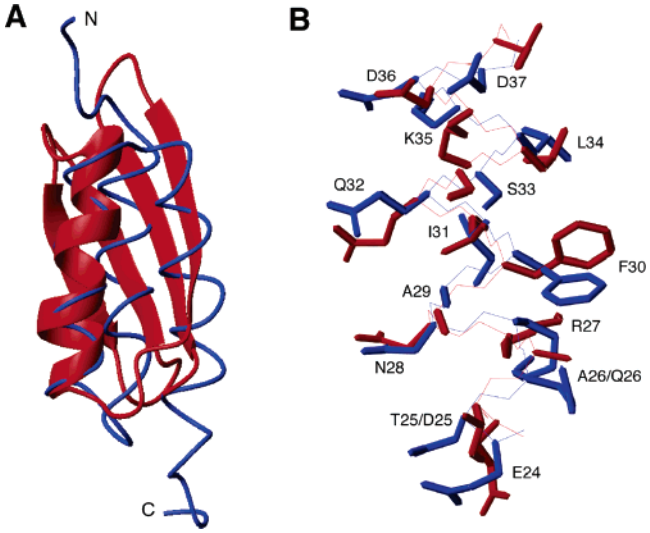

FIGURE 8: (A) Superposition of the G311 (red) and A219 (blue) structures by alignment of the central α-helices. (B) Overlay of the G311 α-helix (red) with A219 helix α2 (blue).

L5V and A34L, are at positions overlapping with the above study. However, it is the introduction of aromatic residues at positions 26, 33, and 34 that appears to play a role in pushing G_{B1} toward the tetrameric structure, and such substitutions were not made in our selection design.

This study differs from other reports on designing homologous heteromorphic proteins in three fundamental ways. First, while other studies have employed computational modeling and intuition to predict the effects of mutating specific residues on structure and stability, the use of phage selection here allows for a more comprehensive search of sequence space. Second, we have been able to generate stable, monomeric mutants utilizing the thermodynamic linkage of folding to biological binding function, in sufficient amounts for detailed structural studies. The other studies that have been done used mostly circular dichroism (CD) spectroscopy and thermal melting to assay whether the protein was folded into a unique, well-defined structure. However, this can be problematic as there are a number of examples in the literature showing that mutants with good CD signals and cooperative thermal transitions do not always have well-dispersed one-dimensional ^{1}H NMR spectra consistent with a folded protein (*31*). Finally, since both G_B and A_B are monomeric, there is no complicating thermodynamic linkage of either structure to a homodimer equilibrium as in the case of ROP (*6*). The G311 and A219 proteins described here and in the accompanying paper therefore provide useful starting points for further quantitative genetic and biophysical studies on principles of folding preferences and conformational switching.

REFERENCES

1. Rose, G. D., and Creamer, T. P. (1994) Protein folding: Predicting predicting, *Proteins 19*, 1−3.
2. Jones, D. T., Moody, C. M., Uppenbrink, J., Viles, J. H., Doyle, P. M., Harris, C. J., Pearl, L. H., Sadler, P. J., and Thornton, J. M. (1996) Towards meeting the Paracelsus Challenge: The design, synthesis, and characterization of paracelsin-43, an α-helical protein with over 50% sequence identity to an all-*β* protein, *Proteins 24*, 502−513.
3. Yuan, S. M., and Clarke, N. D. (1998) A hybrid sequence approach to the paracelsus challenge, *Proteins 30*, 136−143.

4. Dalal, S., Balasubramanian, S., and Regan, L. (1997) Transmuting α helices and β sheets, *Folding Des. 2*, R71−R79.
5. Dalal, S., Balasubramanian, S., and Regan, L. (1997) Protein alchemy: Changing β-sheet into α-helix, *Nat. Struct. Biol. 4*, 548−552.
6. Dalal, S., and Regan, L. (2000) Understanding the sequence determinants of conformational switching using protein design, *Protein Sci. 9*, 1651−1659.
7. Gronenborn, A. M., Filpula, D. R., Essig, N. Z., Achari, A., Whitlow, M., Wingfield, P. T., and Clore, G. M. (1991) A novel, highly stable fold of the immunoglobulin binding domain of streptococcal protein G, *Science 253*, 657−661.
8. Lian, L.-Y., Derrick, J. P., Sutcliffe, M. J., Yang, J. C., and Roberts, G. C. K. (1992) Determination of the solution structures of domains II and III of protein G from *Streptococcus* by ^{1}H nuclear magnetic resonance, *J. Mol. Biol. 228*, 1219−1234.
9. Orban, J., Alexander, P., and Bryan, P. (1992) Sequence-specific ^{1}H NMR assignments and secondary structure of the streptococcal protein G B2-domain, *Biochemistry 31*, 3604−3611.
10. Gallagher, T. D., Alexander, P., Bryan, P., and Gilliland, G. (1994) Two crystal structures of the B1 immunoglobulin-binding domain of streptococcal protein G and comparison with NMR, *Biochemistry 33*, 4721−4729.
11. Derrick, J. P., and Wigley, D. B. (1994) The third IgG-binding domain from streptococcal protein G: An analysis by X-ray crystallography of the structure alone and in a complex with Fab, *J. Mol. Biol. 243*, 906−918.
12. Gouda, H., Torigoe, H., Saito, A., Sato, M., Arata, Y., and Shimada, I. (1992) Three-dimensional solution structure of the B domain of staphylococcal protein A: Comparisons of the solution and crystal structures, *Biochemistry 31*, 9665−9672.
13. Tashiro, M., Tejero, R., Zimmerman, D. E., Celda, B., Nilsson, B., and Montelione, G. T. (1997) High-resolution solution NMR structure of the Z domain of staphylococcal protein A, *J. Mol. Biol. 272*, 573−590.
14. Zheng, D., Aramini, J. M., and Montelione, G. T. (2004) Validation of helical tilt angles in the solution NMR structure of the Z domain of staphylococcal protein A by combined analysis of residual dipolar coupling and NOE data, *Protein Sci. 13*, 549−554.
15. Delaglio, F., Grzesiek, S., Vuister, G. W., Zhu, G., Pfeifer, J., and Bax, A. (1995) NMRPipe: A multidimensional spectral processing system based on UNIX pipes, *J. Biomol. NMR 6*, 277−293.
16. Ikura, M., Kay, L. E., and Bax, A. (1990) A novel approach for sequential assignment of ^{1}H, ^{13}C, and ^{15}N spectra of proteins: Heteronuclear triple-resonance three-dimensional NMR spectroscopy. Application to calmodulin, *Biochemistry 29*, 4659−4667.
17. Grzesiek, S., and Bax, A. (1992) Correlating backbone amide and side chain resonances in larger proteins by multiple relayed triple resonance NMR, *J. Am. Chem. Soc. 114*, 6291−6293.
18. Grzesiek, S., and Bax, A. (1992) Improved 3D triple-resonance NMR techniques applied to a 31 kDa protein, *J. Magn. Reson. 96*, 432−440.
19. Wittekind, M., and Mueller, L. (1993) HNCACB, a high sensitivity 3D NMR experiment to correlate amide-proton and nitrogen resonances with the α and β carbon resonances in proteins, *J. Magn. Reson., Ser. B 101*, 201−205.
20. Grzesiek, S., Anglister, J., and Bax, A. (1993) Correlation of backbone amide and aliphatic side-chain resonances in C-13/N-15-enriched proteins by isotropic mixing of C-13 magnetization, *J. Magn. Reson., Ser. B 101*, 114−119.
21. Montelione, G. T., Lyons, B. A., Emerson, S. D., and Tashiro, M. (1992) An efficient triple resonance experiment using carbon-13 isotropic mixing for determining sequence-specific resonance assignments of isotopically-enriched proteins, *J. Am. Chem. Soc. 114*, 10974−10975.
22. Fesik, S. W., and Zuiderweg, E. R. P. (1988) Heteronuclear three-dimensional NMR spectroscopy: A strategy for the simplification of homonuclear two-dimensional NMR spectra, *J. Magn. Reson. 78*, 588−593.
23. Ikura, M., Kay, L. E., Tschudin, R., and Bax, A. (1990) Three-dimensional NOESY-HMQC spectroscopy of a ^{13}C-labelled protein, *J. Magn. Reson. 86*, 204−209.
24. Brunger, A. T., Adams, P. D., Clore, G. M., DeLano, W. L., Gros, P., Grosse, K. R., Jiang, J. S., Kuszewski, J., Nilges, M., Pannu, N. S., Read, R. J., Rice, L. M., Simonson, T., and Warren, G. L. (1998) Crystallography & NMR system: A new software suite for macromolecular structure determination, *Acta Crystallogr. D54*, 905−921.
25. Cornilescu, G., Delaglio, F., and Bax, A. (1999) Protein backbone angle restraints from searching a database for chemical shift and sequence homology, *J. Biomol. NMR 13*, 289−302.
26. Laskowski, R. A., Rullmann, J. A., MacArthur, M. W., Kaptein, R., and Thornton, J. M. (1996) AQUA and PROCHECK-NMR: Programs for checking the quality of protein structures solved by NMR, *J. Biomol. NMR 8*, 477−486.
27. Lovell, S. C., Davis, I. W., Arendall, W. B., III, de Bakker, P. I., Word, J. M., Prisant, M. G., Richardson, J. S., and Richardson, D. C. (2003) Structure validation by Cα geometry: ϕ, ψ and Cβ deviation, *Proteins 50*, 437−450.
28. Koradi, R., Billeter, M., and Wuthrich, K. (1996) MOLMOL: A program for display and analysis of macromolecular structures, *J. Mol. Graphics 14*, 51−55.
29. Derrick, J. P., and Wigley, D. B. (1992) Crystal structure of a streptococcal protein G domain bound to an Fab fragment, *Nature 359*, 752−754.
30. Kirsten Frank, M., Dyda, F., Dobrodumov, A., and Gronenborn, A. M. (2002) Core mutations switch monomeric protein GB1 into an intertwined tetramer, *Nat. Struct. Biol. 9*, 877−885.
31. Blanco, F. J., Angrand, I., and Serrano, L. (1999) Exploring the conformational properties of the sequence space between two proteins with different folds: An experimental study, *J. Mol. Biol. 285*, 741−753.

BI051232J